Absorption Band Q Model for the Earth

Don L. Anderson and Jeffrey W. Given

Seismological Laboratory
California Institute of Technology
Pasadena, California 91125

August 20, 1981
August 21, 1981
September 22, 1981
September 23, 1981

Abstract

Body wave, surface wave and normal mode data are used to place constraints on the frequency dependence of Q in the mantle. With a simple absorption band, i.e. $Q_s^{-1}(\omega) = q\ (\omega\bar{\tau})$, with $\bar{\tau} = \tau(z)$, the mean relaxation time, being a function of depth (z), it is possible to satisfy the shear sensitive data over a broad frequency range. The quality factor $Q_s(\omega)$ is proportional to ω^{α} in the band and $\omega^{\pm 1}$ at higher and lower frequencies respectively, as appropriate for a relaxation mechanism with a spectrum of relaxation times. The parameters of the band are Q(min) = 80, α = 0.15, and width, 5 decades. The center of the band varies from 10^1 to 1.6×10^3 seconds. The shift of the band with depth is consistent with the expected effects of temperature and pressure. High Q_s regions of the mantle are attributed to a shift of the absorption band to longer periods.

In order to satisfy the gravest fundamental spheroidal modes and the ScS data the absorption band must shift back into the short-period seismic band at the base of the mantle. This may be due to a high temperature gradient or high shear stresses. An attempt is also made to specify bulk dissipation in the mantle and core.

Specific features of the absorption band model are: low-Q in the seismic band at both the top and the base of the mantle, low-Q for long-period body waves in the outer core, an inner core Q_s that increases with period, and low Q_p/Q_s at short periods in the middle mantle. The short-period Q_s increases rapidly at 400 km and is relatively constant from this depth to 2400 km.

Introduction

Attenuation in solids and liquids, as measured by the quality factor Q, is typically frequency dependent. In seismology, however, Q is usually assumed to be independent of frequency. The success of this assumption may be a reflection of the limited precision, resolving power and bandwidth of seismic data.

The theory of seismic attenuation has now been worked out in some detail (Anderson, 1980, Anderson and Minster, 1979, 1980, Minster and Anderson 1980, 1981). Although a mild frequency dependence of Q can be expected over a limited frequency band, Q or Q^{-1} should be a linear function of frequency at greater and lower frequencies.

In this paper we apply the absorption band concept (Liu et al., 1976, Anderson et al., 1977, Anderson and Minster, 1980, Minster and Anderson, 1981) to the attenuation of body waves, surface waves, and free oscillations. The type of data we use is summarized in Anderson and Hart (1978 a,b). The basic method is also described in these papers except that we replace the frequency-independent Q assumption with the absorption band assumption.

The frequency independent Q models, such as SL8 (Anderson and Hart, 1978b) provide an adequate fit to the normal mode data. There is increasing evidence, however, that short-period body waves may require higher Q values (Der and McElfresh 1980, Sipkin and Jordan, 1979, Clements, 1981). Some geophysical applications require estimates of the elastic properties of the Earth outside the seismic band. These include calculations of tidal Love numbers, Chandler periods and high-frequency moduli for comparison with ultrasonic data. The constant-Q models

cannot be used for these purposes. For these reasons it is important to have a physically sound attenuation model for the Earth and this is the primary motivation for the present paper. Our present goal is simply to find out if such a model exists.

Theory

For a solid characterized by a single relaxation time, τ, Q^{-1} is a Debye function with maximum absorption at $\omega\tau = 1$. For a solid with a spectrum of relaxation times the band is broadened and the maximum attenuation is reduced. For a polycrystalline solid with a variety of grain sizes, orientations, and activation energies the absorption band can be appreciably more than several decades wide. If, as seems likely, the attenuation mechanism in the mantle is an activated process the relaxation times should be a strong function of temperature and pressure. The location of the absorption band, therefore, changes with depth. The theory of attenuation in fluids (Anderson, 1980) suggests that Q in the outer core should also depend on frequency.

Theoretical considerations indicate that Q can be a weak function of frequency only over a limited bandwidth. If the material has a finite elastic modulus at high-frequency and a non-zero modulus at low-frequency there must be high- and low-frequency cutoffs in the relaxation spectrum. Physically this means that relaxation times cannot take on arbitrarily high and low values. The relationship between Q and bandwidth (Kanamori and Anderson, 1977) indicates that a finite Q requires a finite bandwidth of relaxation times and therefore an absorption band of finite width. Q can be a weak function of frequency

only in this band.

Anelastic attenuation in solids and liquids having a single characteristic relaxation time satisfies the Debye equation

$$Q^{-1}_{(\omega)} = 2Q^{-1}_{m} \frac{\omega\tau}{1+\omega^2\tau^2} \qquad (1)$$

where Q^{-1}_{m} is the maximum or peak absorption. Crystalline solids typically have a distribution of relaxation times, $D(\tau)$, giving

$$Q^{-1}(\omega) = 2\int_{o}^{\infty} Q^{-1}_{m} D(\tau) \frac{\omega\tau}{1+\omega^2\tau^2} d\tau \qquad (2)$$

For an appropriate choice of $D(\tau)$ this yields an absorption band in which $Q(\omega)$ is slowly varying between τ_1 and τ_2, the minimum and maximum relaxation times in the spectrum. The theory of the absorption band and its relationship to mantle rheology has been developed by Minster and Anderson (1981).

A distribution function of the form

$$D(\tau) \sim \tau^{\alpha-1} \qquad (3)$$

with cutoffs at τ_1 and τ_2 gives

$$Q(\omega) \sim \omega^{\alpha}$$

in the absorption band and $Q(\omega) \sim \omega^{\pm 1}$ outside the band.

We approximate the absorption band in the following way

$$Q = Q_m (f\tau_2)^{-1} \quad , \quad f < 1/\tau_2$$

$$Q = Q_m (f\tau_2)^{\alpha} \quad , \quad 1/\tau_2 < f < 1/\tau_1$$

$$Q = Q_m (\tau_2/\tau_1)^{\alpha} (f\tau_1), \quad f > 1/\tau_1$$

where f is the frequency, τ_1 is the short-period cutoff, τ_2 is the long-period cutoff and Q_m is the minimum Q which occurs at $f = 1/\tau_2$. These parameters are shown in Figure 1.

Effect of T, P and Stress

The relaxation time, τ, for an activated process, depends exponentially on temperature and pressure:

$$\tau = \tau_o (z) \exp [(E^* + PV^*)/RT]$$

where E^* and V^* are activation energy and volume respectively. The characteristic time τ_o depends on ℓ^2 and D for diffusion controlled mechanisms where ℓ and D are a characteristic length and a diffusivity, respectively. Characteristic lengths, such as dislocation or grain size, are a function of tectonic stress which is a function of depth, Z.

The location of the band, therefore, depends on stress, temperature and pressure. The width of the band is controlled by the distribution of relaxation times which in turn depends on the distribution of grain sizes or dislocation lengths.

With an activation energy of 60 kcal/mole, τ decreases by about an order of magnitude for a temperature rise of 200° C. An activation volume of 10 cm^3/mole causes τ to increase by an order of magnitude for a 30 kbar increase in pressure. In regions of low temperature gradient the maximum absorption shifts to longer periods with increasing depth. Characteristic lengths such as grain size and dislocation length decrease with increasing stress. A decrease in tectonic stress by a factor of three increases the relaxation time by an order of magnitude. A decrease of stress with depth is expected to move the absorption band to longer periods.

The effect of pressure dominates over temperature for most of the upper mantle (Minster and Anderson, 1981) and tectonic stress probably decreases with depth. Therefore the absorption band is expected to move to longer periods with increasing depth. A reversal of this trend may be caused by high-stress or high- temperature gradients in internal boundary layers, or by enhanced diffusion due to changes in crystal structure or in the nature of the controlling point defects.

Procedure

The parameters of the absorption band are 1.) minimum Q, (Q_m) 2.) short-period corner frequency, (τ_1) 3.) long-period corner frequency, (τ_2) and 4.) the frequency dependency of Q in the absorption band, i.e.

$Q \sim \omega^{\alpha}$. For a given physical mechanism there are relationships between the width of the band, (τ_2/τ_1), Q_m and α, i.e. these three parameters are not independent (Minster and Anderson, 1981). For fixed α, τ_2/τ_1 increases as Q_m^{-1} decreases. We assume that the parameters of the absorption band, Q_m^{-1}, τ_1/τ_2 and α are fixed throughout the mantle and use the seismic data to determine the location of the band as a function of depth, i.e. $\tau_1(z)$. This assumption is equivalent to assuming that the activation energy, E^*, and activation volume, V^*, are fixed. By assuming that the characteristics of the absorption band are invariant with depth we are assuming that 1.) the same mechanism or class of mechanisms is responsible for attenuation throughout the mantle and 2.) the width of the band is controlled by a distribution of characteristic relaxation times rather than a distribution of activation energies. Although these assumptions can be defended to some extent they have been introduced to reduce the number of model parameters.

In setting up the starting model we used the following considerations:

1. Body waves traverse the lowermantle with relatively little attenuation. On the other hand, the normal modes require a low-Q lowermantle. This suggests that the absorption band in the lower mantle is centered at long periods.

2. The uppermantle is highly attenuating for both surface waves and body waves although there is some evidence for an increase in Q at very short periods. The absorption band in the uppermantle therefore occurs

at shorter periods than in the lowermantle but τ_1 is larger than the periods of high-frequency body waves.

3. At body-wave periods the Q is large in the outer core and small in the inner core. We assume that the short-period Q decreases with depth, throughout the core.

4. The observation of core modes requires that Q of the inner core be high at normal-mode periods. The radial modes imply a high-Q outer core. We assume, therefore, that the core behaves as a classic fluid, with $Q \sim \omega^{-1}$, at long periods.

Q_m is found from the minimum Q modes, i.e. mantle Love and Rayleigh waves and is assumed to be constant with depth. The parameters α and τ_1 were estimated from data that sample the mid-mantle at various frequencies. This part of the mantle is high-Q for body waves but low-Q at normal-mode periods. This suggests that the high- frequency end of the band occurs at intermediate periods. In order to satisfy the relatively low-Q of long-period ScS, the absorption band has to be shifted to higher frequencies at the base of the mantle. τ_2 is then determined from ${}_oS_2$ to ${}_oS_5$ which are sensitive to Q_β at the base of the mantle. With Q_m, α, τ_1, and τ_1/τ_2 fixed the full dataset is used to adjust $\bar{\tau}$, i.e. the location of the absorption band as a function of depth. The fixed parameters of the band are $\alpha = 0.15$ and $Q_m = 80$. A similar procedure is used to estimate Q_β in the inner core. The parameters of the absorption bands are given in Table 1. The locations of the bands as a function of depth are shown in Figures 2 to 4. We

will refer to the Absorption Band Model as ABM.

The Mantle

The variation of τ_1 and τ_2 with depth in the mantle is shown in Figure 2. Note that τ decreases with depth in the uppermost mantle. This is expected in regions of high thermal gradient. τ increases slightly below 250 km and abruptly at 400 km. In the early iterations it was assumed that any abrupt change in τ would occur at 670 km but this is clearly too deep. Apparently, a high temperature gradient and high tectonic stresses can keep the absorption band at high frequencies throughout most of the uppermantle but these effects are overridden below 400 km where most mantle minerals are in the cubic structure. A phase change, along with high pressure and low stress, may contribute to the lengthening of the relaxation times. Note that τ changes only slightly through most of the lowermantle.

The location of the absorption band is almost constant from a depth of about 400 to 2000 km (Figure 2). This gives high-Q_s for body waves and low-Q_s for free oscillations. However, the low order spheroidal modes require a distinctly higher Q in the lower 500 km of the mantle. These data can be satisfied by moving the band to the location shown in the lower part of Figure 3. This gives a low Q region at the base of the mantle at body wave periods (region "D" in Figure 4).

The parameter α was initially set to 0.3 but we were not able to match the data with this strong a frequency dependence in the absorption band. We found that $\alpha = 0.15$ gave a satisfactory fit.

The Core

Under normal conditions fluids in general, and molten metals in particular, satisfy the relaxation equations with $\omega\tau << 1$ giving $Q \sim \omega^{-1}$. Pressure serves to increase τ and the high absorption of short-period P-waves in the inner core suggests that τ may be of the order of 1 second in this region (Anderson, 1980). The high-Q of the outer core at body wave frequencies suggests that the absorption band is at longer or shorter periods.

Q in the core is assumed to be a Debye peak which we approximate as a narrow absorption band with a fixed Q_m and width. With these assumptions we find $Q_m = 400$ and $\bar{\tau}$, the mean relaxation time, decreases with depth from 32 to 19 seconds in the outer core to 6 seconds in the inner core.

The net result is a slowly varying Q (406 to 454) for the inner core between 0.1 to 10 seconds increasing to 3320 at 100 seconds and 3.3×10^4 at 1000 seconds. In the outer part of the outer core Q decreases from 7530 at 1 second to 753 at 10 seconds and then increases to 6000 at 1000 seconds. The relative location of the band is fixed by the observation that short period P-waves see a high-Q outer core and a low-Q inner core. The absorption band model predicts relatively low Q for 10-50 second P-waves in the outer core. Data is sparse but long-period P-waves in the outer core may be attenuated more than short-period waves (Suzuki and Sato, 1970, Qamar and Eisenberg, 1974). There are, however, complications in trying to interpret this data (Cormier and Richards, 1976, Choy, 1977).

Bulk Attenuation

The attenuation of shear waves, Love and Rayleigh waves, toroidal oscillations and most of the spheroidal modes are controlled almost entirely by Q_s in the mantle. Once the mantle Q_s is determined the Q of P-waves and the high-Q spheroidal and radial modes are used to estimate Q_K.

The relationship between Q_p, Q_s and Q_K is

$$Q_p^{-1} = L\, Q_s^{-1} + (1 - L)\, Q_K^{-1}$$

where $L = (4/3)\,(\beta/\alpha)^2$ and β and α are the shear and compressional velocities. For a Poisson solid with $Q_K^{-1} = 0$

$$Q_p = (9/4)\, Q_s$$

There is a small component of bulk dissipation associated with the shear deformation of polycrystalline material (Budiansky and O'Connell, 1980). This amounts to about 2% of the shear dissipation and has the same frequency dependence. There is also a component of bulk dissipation in such material that is independent of the shear dissipation and which can be much larger. This is the intergranular thermoelasticity mechanism (Zener, 1948), a relaxation mechanism that depends on grain size and thermal conductivity and is only a weak function of temperature and pressure. This mechanism is predicted to be important at body wave frequencies (Anderson, 1980).

In fluids, bulk dissipation is controlled by viscosity and

concentration fluctuations (Anderson, 1980) and, again, the classic relaxation relations hold. Therefore, the absorption band concept can be applied to bulk dissipation in both the mantle and core.

The main constraints on the bulk attenuation are provided by the low-order radial modes, the high-Q spheroidal modes, and short-period compressional waves. Bulk losses caused by bulk viscosity or intergranular thermal currents are relaxation mechanisms and, therefore, $Q_K \sim \omega^{-1}$ at long-periods.

In general, bulk attenuation is less important than shear attenuation. The radial mode ${}_0S_0$ apparently requires bulk dissipation somewhere in the Earth at a period of 1230 seconds (Anderson and Hart, 1978a,b; Sailor and Dziewonski, 1978). We assume that free oscillation periods are long compared to bulk relaxation times (Anderson, 1980) and, therefore, $Q \sim \omega^{-1}$. The value of Q_K at long-periods is estimated from the radial modes. With this procedure, however, the predicted Q_p for short-period body waves is distinctly too low. This implies that the minimum absorption, in the context of an absorption band model, occurs somewhere between the body wave and normal mode bands. By trial and error we found that a minimum Q_K of 400 could satisfy P-wave observations for both the inner core and uppermantle. We adopted this value for the whole Earth and found the location of the Q_K band. The values for τ_2, with this assumption, ranged from 0.2 to 67 seconds.

The variation of Q_K with frequency for the various regions of the Earth is shown in Figure 5. The location of the lowermantle curve is dictated by the observation that both short-period P-waves and the radial modes require a high-Q lowermantle. Low-Q is predicted in this

region for higher high-frequency P-waves.

A useful measure of body-wave attenuation is the ratio of travel time to average Q along the path, or t* (Kovach and Anderson, 1964). If t_p^* at short distances is to be as great as 0.6 to 1.0 sec then a compressional component of attenuation is required. With the Q_K band as shown, the t_p^* at 1 sec period and 30° distance is 0.65 sec. No attempt was made to estimate τ_1, i.e. the short-period Q_K^{-1} rolloff, for the mantle. This requires knowledge of Q_p as a function of frequency for periods shorter than about 1 sec. If we assume that Q_K of the uppermantle is a simple Debye peak then $Q_K \sim \omega$ at periods shorter than about 1 sec. On the other hand τ_1 for Q_s in the uppermantle is about 0.3×10^{-2} to 10^{-3} sec so that Q_p increases linearly with frequency only at very short periods.

The location of the Q_K band for the inner core is constrained by the low-Q_p for short-period P-waves. Q_K of the outer core is constrained by P-waves and the radial modes. Note that Q_K, and therefore Q_p, is predicted to increase with period from about 50 seconds to longer periods. Relatively low Q, < 500, is predicted between about 10 and 80 seconds. Measurements of the attenuation of long-period body waves in the outer core would be a severe test of the suggested location of the Q_K band.

Results

Tables 5 - 10 and Figure 6 give the calculated Q for ABM and two frequency independent Q models (SL8, Anderson and Hart, 1978, PREM, Dziewonski and Anderson, 1981). The main differences of the absorption

band model, compared with the constant-Q models, are the higher theoretical values for ${}_oS_2$, ${}_oS_3$ and ${}_oS_4$ and the more rapid decrease of Q from ${}_oS_5$ to ${}_oS_{10}$. Unfortunately, there is considerable uncertainty in the Q values for the low order spheroidal modes. The data are compiled from Anderson and Hart (1978a,b), Chael and Anderson (1981), Nakanishi (1979a), and Dziewonski and Steim (1981). In general, the fit of ABM is as good as, or better than, the constant Q models.

The fundamental toroidal modes are given in Table 8. ABM has values appreciably higher than SL8 and PREM for modes ${}_oT_3$ to ${}_oT_{20}$. The toroidal overtones are given in Table 9.

The values for t^*_p and t^*_s (travel time over average Q) are given in Table 11 as a function of distance and period. At 100 sec the Q_K contribution is small and t^*_p ~1 and t^*_s ~ 4-5, values which are commonly used in long-period waveform fitting. At high frequencies the t* values are much lower, consistent with spectral studies (Der and McElfresh, 1980). Note that $t^*_s < 4\ t^*_p$ at short periods because of the Q_K contribution. If there were no bulk absorption t^*_p (30°) at 1 sec would be 0.32 sec and the other t^*_p values at short period would be correspondingly reduced. Note that t* decreases gradually with frequency at the shorter distances. The study of t* as a function of frequency and distance should allow better constraints to be placed on τ_1, for both Q_s and Q_K, as a function of depth.

The average Q values for the crust and uppermantle (<670 km), lowermantle (>670 km) and whole mantle are given in Table 3 and, for Q_s, in Figure 7. Figure 7 also gives observed Q values for ScS; these are estimates of whole mantle Q_s. Table 3 also gives the average Q of a ${}_oS_2$

type mode at tidal and Chandler periods ignoring rigid body rotation.

We conclude that ABM is an adequate fit to a variety of data over a broad frequency band. The constant Q assumption, therefore, is not required by the data.

Discussion

The absorption band for Q_s is centered at about 1 sec period in the upper 400 km of the mantle with the maximum absorption at about 100 seconds. The band moves slightly to longer periods with increasing depth over this interval. This could be due to the effect of increasing pressure and decreasing stress. The band jumps to longer periods at about 400 km depth and gradually moves to longer periods with increasing depth. The location of the band in the lowermantle is determined from the long period spheroidal modes. The very low- order spheroidal modes, ${}_oS_2$ to ${}_oS_5$, can only be satisfied by moving the absorption band back to shorter periods at the base of the mantle.

Our goal was to determine if a physically realistic model of the absorption band, with its attendant frequency dependence and large shifts with depth, could explain the surface wave and normal mode absorption spectrum. This goal was achieved. The absorption band is centered in the seismic band in the upper 400 km of the mantle and then shifts rapidly to longer periods in the lower mantle. This is the effect expected at high pressure and low stress. The absorption band shifts back to higher frequencies at the base of the mantle (region D"). This may be due to a high temperature gradient or high stresses in D", effects expected in a thermal and mechanical boundary layer at the base

of a convecting mantle.

There is much less control on Q_K. The assumption that bulk losses also satisfy the relaxation relations and that the Q_K absorption band is centered at short periods leads to the conclusion that the minimum Q_K is greater than the minimum Q_s. The outer core may have relatively high absorption for long-period body waves. With the placement of the Q_K band $Q_p < Q_s$ at short periods at midmantle depths. This conclusion, however, rests on the assumption that $t^*_p > 0.6$ sec at short periods. Unfortunately, global averages for t^*_p and t^*_s are not available. If t^*_p(1 sec) is about 0.3 sec then there is no need for bulk attenuation at short periods.

Since most seismic data averages over a large part of the mantle or core the integrated effect leads to a mild frequency dependence over most of the seismic band. A stronger frequency dependence is predicted for the high-Q regions of the Earth. The deformational Q at tidal and Chandler periods is predicted to be somewhat less than for the mode ${}_0S_2$. The actual Q of the Chandler wobble, however, is greater because of rigid body rotation effects.

There is obviously much more to be done in the exploration of the new model space opened up by the absorption band concept. ABM satisfies the available data but we have not discussed resolving power or uniqueness of the model. Such discussions ignore the assumptions which go into setting up the inversion procedure and which are as important as the data itself. For example, Earth models resulting from the inversion of normal mode data allowing for anisotropy and anelastic dispersion (e.g., Dziewonski and Anderson, 1981) are quite different from those

which ignore these effects even if the same dataset is used. The assumptions and parameterizations are different and therefore the models are different. In addition, since $\omega(Q)$ is double valued, the present problem is intrinsically non-linear, i.e. a given $Q(z)$ can be achieved at two distinct locations on the absorption band. From our parametric investigations we feel that the general locations of the Q_s bands are proper and that the resolving lengths are of the order of 200-500 km in the upper and lowermost mantle. Because of the lack of data there is very little control on the parameters or locations of the Q_K bands. However, once we assume that the Q_K absorption bands are on the high frequency side of the normal mode band, the parameters can be determined. The alternative assumption cannot be ruled out with the present data. We need more high-accuracy data particulary for the low-order spheroidal modes, overtones and toroidal modes, and for long-period P-waves in the outer core.

Acknowledgments

We thank Robert Hart for use of a computer program. Thorne Lay, Bernard Minster, Anton Hales and Ichino Nakanishi reviewed the manuscript and provided helpful comments. This research was supported by the Earth Sciences Section National Science Foundation Grant No and EAR77-14675 and National Aeronautics and Space Administration Grant No. NSG-7610, Contribution Number 3695, Division of Geological and Planetary

Sciences, California Institute of Technology, Pasadena, California 91125.

Figure Captions

Figure 1. Schematic illustration of the absorption band. For shear wave attenuation in the mantle Q_m, α and τ_2/τ_1 are fixed and τ_1 is found as a function of depth from the seismic data.

Figure 2. τ_1 and τ_2 as a function of depth in the mantle for the Absorption Band Model (ABM).

Figure 3. The location of the absorption band for Q_s as a function of depth in the mantle.

Figure 4. Q_s as a function of period for the mantle and inner core for ABM. Note the similarity of the uppermantle and the lowermost mantle ("D"). These may be thermal (high-temperature gradient) and mechanical (high-stress) boundary layers associated with mantle convection.

Figure 5. Q_K as a function of frequency for various regions in the Earth. There are two layers in the outer core (see Table 4).

Figure 6. Comparison of calculated Q values for ABM and two frequency independent Q models, SL8 and PREM. The approximate range of the data for the fundamental modes is shown by vertical bars.

Figure 7. Data for Q_{ScS} as a function of period (Anderson and Hart, 1978a; Jordan and Sipkin, 1977; Sipkin and Jordan, 1979; Nakanishi, 1979b). Also shown are average Q_s values for the lowermantle, uppermantle and whole mantle for ABM. The whole mantle curve corresponds to ScS.

References

Anderson, Don L., Bulk attentuation in the Earth and viscosity of the core, Nature, 285, 204-207, 1980.

Anderson, Don L. and R. S. Hart, Attenuation models of the earth, Phys. Earth Planet. Inter., 16, 289-306, 1978a.

Anderson, Don L. and R. S. Hart, Q of the Earth, J. Geophys. Res., 83, 5869-5882, 1978b.

Anderson, Don L. and J. B. Minster, The frequency dependence of Q in the Earth and implications for mantle rheology and Chandler wobble, Geophys. J. R. astr. Soc., 58, 431-440, 1979.

Anderson, Don L. and J. B. Minster, Seismic velocity, attenuation and rheology of the uppermantle, in Source Mechanism and Earthquake Prediction, C. J. Allègre (ed.), 13-22, 1980.

Anderson, Don L., H. Kanamori, R. S. Hart and H. -P. Liu, The Earth as a seismic absorption band, Science, 196, 1104-1106, 1977.

Budiansky, B. and R. J. O'Connell, Bulk attenuation in heterogeneous media, Solid Earth Geophysics and Geotechnology, S. Nemat-Nasser (ed)., Am. Soc. M. Eng., 1980.

Chael, E. and Don L. Anderson, Global Q estimates from antipodal Rayleigh waves, (in press).

Clements, J., Intrinsic Q and its frequency dependence, Phys. Earth Planet. Interiors

Choy, G., Theoretical seismograms of core phases calculated by frequency-dependent full wave theory, and their interpretation, Geophys. J. R. astron. Soc., 51,

275-312, 1977.

Cormier, V. and P. Richards, Comments on "The damping of core waves" J. Geophys. Res., 81, 3066-3068, 1976.

Der, Z. and T. W. McElfresh, Time domain methods, the values of t_p^* and t_s^* in the short-period band and regional variations of the same across the United States, Bull. Seism. Soc. Am., 70, 921-924, 1980.

Dziewonski, A. and Don L. Anderson, Preliminary reference Earth model, Phys. Earth Planet. Int., 25, 297-356, 1981.

Dziewonski, A. and J. Steim, Dispersion and attenuation of mantle waves through wave-form inversion, Geophys. J. R. astron. Soc. (in press).

Jordan, T. and S. Sipkin, Estimation of the attenuation operator for multiple ScS waves, Geophys. Res. Lett., 4, 167-170, 1977.

Kanamori, H. and Don L. Anderson, Importance of physical dispersion and in surface-wave and free oscillation problems, Review, Rev. Geophys. Space Sci. 15, 105-112, 1977.

Kovach, R. L. and Don L. Anderson, Attenuation of shear waves in the upper and lowermantle, Bull. Seism. Soc. Am., 54, 1855-1865, 1964.

Liu, H. -P., Don L. Anderson and H. Kanamori, Velocity dispersion due to an elasticity; implications for seismology and mantle composition, Geophys. J. R. astron. Soc., 47, 41-58, 1976.

Minster, J. B. and Don L. Anderson, Dislocations and nonelastic processes in the mantle, J. Geophys. Res., 85, 6347-6352,

1980.

Minster, J. B. and Don L. Anderson, A model of dislocation-controlled rheology for the mantle, Phil. Trans. Roy. Soc. (London), 299, 319- 356, 1981.

Nakanishi, I., Phase velocity and Q of mantle Rayleigh waves, Geophys. J. R. astron. Soc., 58, 35-59, 1979a.

Nakanishi, I., Attenuation of multiple ScS waves beneath the Japanese arc, Phys. Earth Planet. Inter., 19, 337-347, 1979b.

Qamar, A. and A. Eisenberg, The damping of core waves, J. Geophys. Res., 79, 758-765, 1974.

Sailer, R. and A. Dziewonski, Measurements and interpretation of normal mode attentuation, Geophys. J. R. astron Soc., 53, 559-582, 1978.

Sipkin, S. A. and T. H. Jordan, Frequency dependence of Q_{ScS}, Bull. Seism. Soc. Am., 69, 1055-1079, 1979.

Suzuki, Y. and R. Sato, Viscosity determination in the Earth's outer core from ScS and SKS phases, J. Phys. Earth, 18, 15-170, 1970.

Zener, C., Elasticity and Anelasticity of metals, J. Chicago Press, Chicago, Illinois, 1948.

Table 1
Absorption band parameters for Q_s

Radius (km)	τ_1 (sec)	τ_2/τ_1	Q_s(min) (τ_1)	Q_s (100^s sec)	α
1230	0.14	2.43	35	1000	0.15
3484	-	-	-	-	-
4049	0.0025	10^5	80	92	0.15
4832	25.2	10^5	80	366	0.15
5700	12.6	10^5	80	353	0.15
5950	0.0031	10^5	80	330	0.15
6121	0.0009	10^5	80	95	0.15
6360	0.0044	10^5	80	90	0.15
6371	0	-	500	500	0

Table 2

Relaxation times (τ_1, τ_2) and Q_K for bulk attenuation at various periods
Q_K (min) = 400, a = 0.15

	τ_1 (sec)	τ_2 (sec)	Q_K T (sec) 1	10	100	1000
upper mantle	0	3.33	479	1200	1.2×10^4	1.2×10^5
lower mantle	0	0.20	2000	2×10^4	2×10^5	2×10^6
outer core	15.1	66.7	7530	753	600	6000
	9.04	40.0	4518	493	1000	10,000
inner core	3.01	13.3	1506	418	3000	3×10^4

Table 3
Average mantle Q values as function of period, Model ABM

	Period, s					
	0.1	1.0	4.0	10.0	100	1000
			Q_s			
UPPER MANTLE	379	267	210	173	127	2..
LOWER MANTLE	1068	721	520	382	211	266
WHOLE MANTLE	691	477	360	280	176	274
			Q_p			
UPPER MANTLE	513	362	315	354	311	727
LOWER MANTLE	586	1228	1262	979	550	671
WHOLE MANTLE	562	713	662	639	446	687

	$Q\ ({}_oS_2)$		
${}_oS_2$	3232 sec	12 hrs	14 mos
	596	514	463

Table 4
Q_s and Q_p as function of depth and period for model ABM

	Q_s				Q_p			
Depth (km)	1 (sec)	10 (sec)	100 (sec)	1000 (sec)	1 (sec)	10 (sec)	100 (sec)	1000 (sec)
5142	100	1000	10,000	10^5	511	454	3322	3.3×10^4
4044	-	-	-	-	4518	493	1000	10^4
2887	-	-	-	-	7530	753	600	6000
2843	184	130	92	315	427	345	247	846
2400	184	130	92	315	427	345	247	846
2200	11,350	1135	366	259	2938	2687	942	668
671	8919	892	353	250	2921	2060	866	615
421	5691	569	330	234	741	840	819	603
421	190	134	95	254	302	296	244	659
200	157	111	90	900	270	256	237	2365
11	200	141	100	181	287	262	207	377
11	500	500	500	500	487	767	1168	1232

Table 5
Fundamental spheroidal mode Q

MODE	PERIOD, S	ABM	SL8	PREM	DATA
${}_oS_2$	3232	596	540	510	500-589
${}_oS_3$	2134	499	435	417	450-520
${}_oS_4$	1546	421	398	373	400-411
${}_oS_5$	1190	377	391	356	300-400
${}_oS_6$	964	350	391	347	343-399
${}_oS_7$	812	333	392	342	373-460
${}_oS_8$	708	323	388	337	295-357
${}_oS_9$	634	319	380	333	328
${}_oS_{10}$	580	319	368	328	320
${}_oS_{12}$	503	317	341	315	308
${}_oS_{14}$	448	307	313	298	294
${}_oS_{16}$	407	294	286	279	276
${}_oS_{18}$	374	276	262	259	282
${}_oS_{20}$	347	254	241	241	240
${}_oS_{22}$	325	231	222	225	228
${}_oS_{24}$	306	212	207	211	210
${}_oS_{26}$	290	198		200	198
${}_oS_{28}$	275	187		191	188
${}_oS_{30}$	262	177		183	179
${}_oS_{40}$	212	148	149	158	151
${}_oS_{50}$	178	136	136	143	137
${}_oS_{60}$	153	128	129	133	122
${}_oS_{70}$	134	121	125	126	120

Table 5 A
Fundamental spheroidal mode Q
(continued)

MODE	PERIOD,S	ABM	SL8	PREM	DATA
$_0S_{76}$	125	117			122
$_0S_{80}$	119	114		122	
$_0S_{90}$	107	107		119	
$_0S_{100}$	97	100		118	
$_0S_{110}$	88	93		118	
$_0S_{120}$	81	94		119	
$_0S_{130}$	75	95		121	
$_0S_{140}$	70	96		124	
$_0S_{150}$	66	97		128	

Table 6
Spheroidal overtone Q

MODE	PERIOD, S	ABM	SL8	PREM	DATA
$_1S_2$	1470	343			
$_1S_4$	852	296			
$_1S_7$	604	315	473		484
$_1S_{10}$	466	261			
$_1S_{20}$	254	163			
$_1S_{40}$	149	157			
$_1S_{50}$	125	151			
$_2S_2$	1049	6563			546
$_2S_4$	726	411	544	380	350-546
$_2S_{10}$	416	221		181	
$_2S_{15}$	309	161	252	258	244
$_2S_{23}$	202	118	407		514
$_2S_{26}$	179	191	202	194	158-275
$_2S_{30}$	161	200	179	181	150-207
$_2S_{31}$	157	198	178	179	143
$_2S_{39}$	131	188	169	168	179
$_2S_{57}$	98	170	160		174
$_2S_{60}$	94	165	158	154	151
$_3S_1$	1061	856	902	827	1020
$_3S_2$	903	577		367	
$_3S_6$	392	212		276	
$_3S_{12}$	297	210	261	245	179-239
$_3S_{13}$	285	214	255	241	227-271
$_3S_{20}$	217	222	212	210	229
$_3S_{42}$	111	206	211	225	180

Table 7
Spheroidal overtone Q

MODE	PERIOD, S	ABM	SL8	PREM	DATA
$_4S_3$	488	465	534	480	560
$_4S_{14}$	225	189	296	264	288
$_4S_{19}$	192	218	294	259	291
$_4S_{21}$	181	231	291	259	275
$_4S_{23}$	170	241	287	259	312
$_4S_{25}$	161	248	281	258	260
$_4S_{26}$	157	250	278	256	306
$_4S_{31}$	139	246	258	252	264
$_4S_{32}$	136	244	254	251	299
$_4S_{34}$	130	237	245	246	234
$_4S_{35}$	127	234	240	244	246
$_4S_{39}$	118	218	223	233	193
$_5S_7$	304	480	-	493	496
$_5S_{22}$	154	212	303	-	306
$_5S_{25}$	143	227	294	263	231
$_5S_{26}$	140	233	291	260	236
$_5S_{30}$	129	251	276	248	248
$_5S_{38}$	110	265	263	235	223
$_6S_1$	505	695	873	-	700
$_6S_8$	268	189	263	-	286
$_6S_9$	252	229	314	321	292
$_6S_{13}$	191	208	264	-	291
$_6S_{23}$	138	272	325	292	299
$_6S_{31}$	116	259	244	252	391
$_6S_{36}$	106	282	247	250	342
$_6S_{47}$	89	263	237	245	276

Table 8

Fundamental toroidal mode Q

MODE	PERIOD, S	ABM	SL8	PREM	DATA
${}_0T_2$	2631	268	272	250	250-400
${}_0T_3$	1702	269	257	240	325-400
${}_0T_4$	1304	267	241	228	290-425
${}_0T_5$	1076	265	224	216	185-280
${}_0T_6$	926	263	209	205	266-357
${}_0T_7$	818	259	195	196	125-141
${}_0T_8$	736	253	184	187	170-295
${}_0T_9$	672	246	175	180	157-180
${}_0T_{10}$	619	238	167	173	188-250
${}_0T_{12}$	538	219	155	163	189-220
${}_0T_{14}$	477	200	145	155	200-270
${}_0T_{16}$	430	184	139	149	168-215
${}_0T_{20}$	360	160	129	142	175-249
${}_0T_{25}$	300	142	123	137	110-149
${}_0T_{30}$	258	136	119	134	111-142
${}_0T_{40}$	201	127	114	131	102-133
${}_0T_{50}$	164	119	112	131	108-130
${}_0T_{60}$	139	112	111	132	104-116
${}_0T_{70}$	121	105	111	---	100
${}_0T_{80}$	107	98	111	---	86-121
${}_0T_{85}$	101	95	111	---	108
${}_0T_{110}$	79	90	111	---	109

Table 9

Toroidal overtone Q

MODE	PERIOD,S	ABM	SL8	PREM	DATA
$_1T_7$	475	224	262	237	238
$_1T_{12}$	340	217	232	217	195
$_1T_{19}$	249	212	204	203	195
$_1T_{25}$	206	203	184	187	192
$_1T_{62}$	107	135	---	140	138
$_2T_{36}$	133	228	214	204	183
$_2T_{46}$	112	206	190	189	189
$_2T_{49}$	107	198	181	183	207
$_2T_{54}$	100	186	172	173	144
$_2T_{62}$	91	168	159	159	143
$_3T_{26}$	147	243	241	220	264
$_3T_{27}$	144	246	240	---	296
$_3T_{30}$	134	251	239	219	215
$_3T_{53}$	91	215	214	---	236
$_4T_{11}$	200	160	247	221	208
$_4T_{17}$	170	146	254	---	204

Table 10

High Q modes

	T (Sec)	ABM	SL8	PREM	DATA
$_1S_7$	604	315	473	372	484
$_2S_4$	725	411	---	380	350
$_3S_1$	1061	856	902	827	1020
$_4S_3$	488	466	534	---	560
$_4S_{23}$	170	241	287	---	312
$_4S_{26}$	157	250	278	---	306
$_5S_7$	304	480	589	493	496
$_6S_1$	505	695	873	---	700
$_oS_0$	1230	6107	4374	5328	5230
$_1S_0$	614	1293	1180	1499	1970
$_2S_0$	399	1243	1024	1241	1170
$_3S_0$	306	873	851	1083	874
$_4S_0$	244	862	945	969	989
$_5S_0$	205	782	947	921	824
$_6S_0$	174	689	1057	913	933

Table 11

t_P^* and t_S^* as function of distance and period for Models ABM and the frequency independent Q Model SL8

Period (sec)		Distance (degrees) 30	40	50	60	70	80	90
0.1	P	0.61	0.72	0.83	0.93	1.02	1.10	1.51
	S	0.99	0.97	0.93	0.89	0.87	0.85	1.97
1.0	P	0.65	0.67	0.66	0.65	0.66	0.67	1.14
	S	1.44	1.43	1.39	1.34	1.32	1.29	2.87
4.0	P	0.73	0.74	0.71	0.69	0.68	0.67	1.23
	S	1.93	1.97	1.96	1.95	1.93	1.91	3.81
10.0	P	0.68	0.71	0.72	0.71	0.72	0.72	1.32
	S	2.52	2.66	2.75	2.81	2.81	2.84	4.91
100.0	P	0.86	0.96	1.02	1.07	1.13	1.17	1.92
	S	3.82	4.22	4.55	4.84	5.10	5.35	8.00
				MODEL SL8				
	P	0.91	1.02	1.04	1.04	1.06	1.06	1.12
	S	4.15	4.61	4.77	4.82	4.93	4.99	5.07

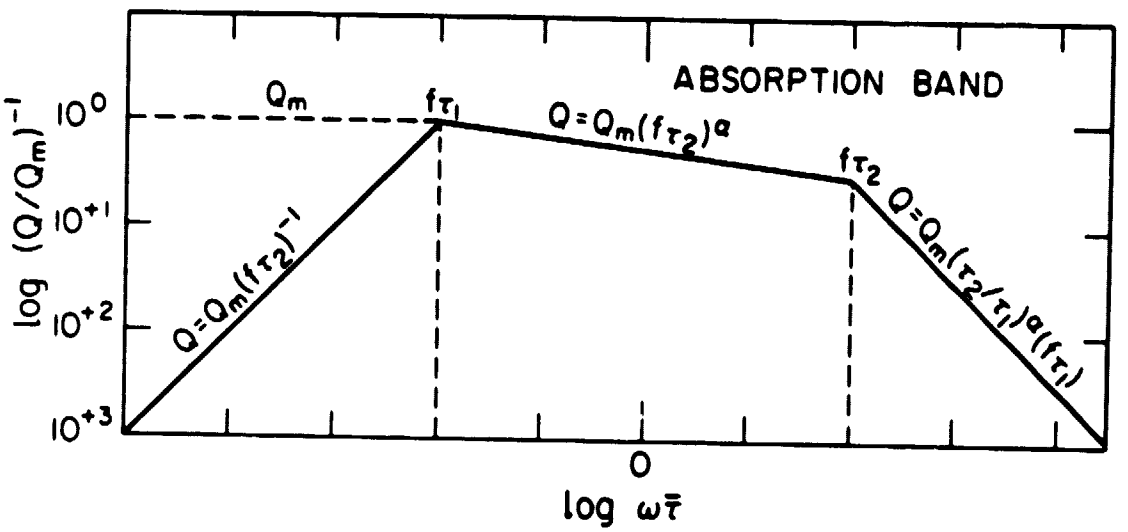
ABSORPTION BAND
Q_m
$f\tau_1$
$Q=Q_m(f\tau_2)^{\alpha}$
$f\tau_2$
$Q=Q_m(\tau_2/\tau_1)^{\alpha}(f\tau_1)$
$Q=Q_m(f\tau_2)^{-1}$
10^0
10^{+1}
10^{+2}
10^{+3}
$\log (Q/Q_m)^{-1}$
0
$\log \omega\bar{\tau}$

Fig. 1

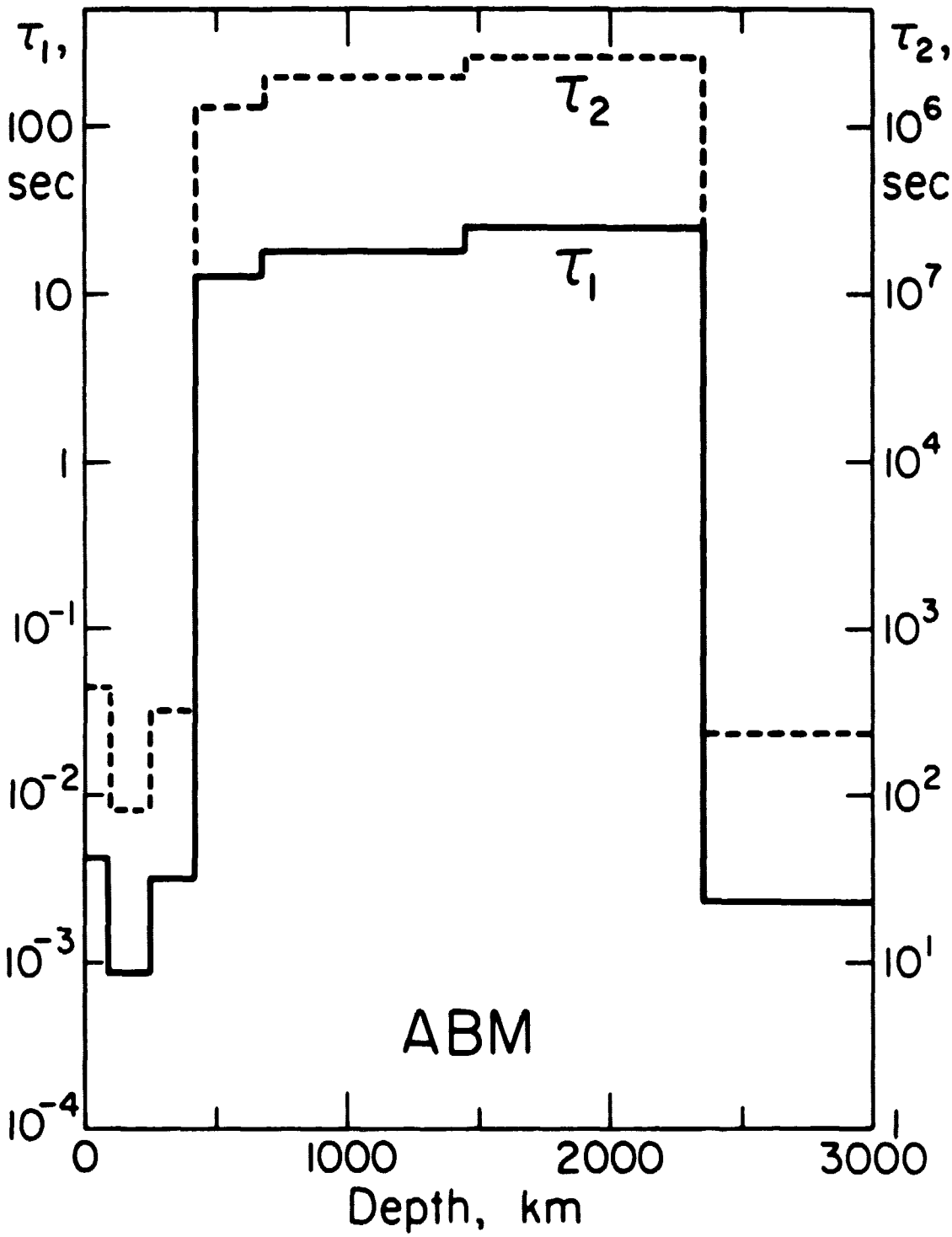
τ_1,
100
sec
10
1
10^{-1}
10^{-2}
10^{-3}
10^{-4}
τ_2,
10^6
sec
10^7
10^4
10^3
10^2
10^1
1
τ_2
τ_1
ABM
0
1000
2000
3000
Depth, km

Fig. 2

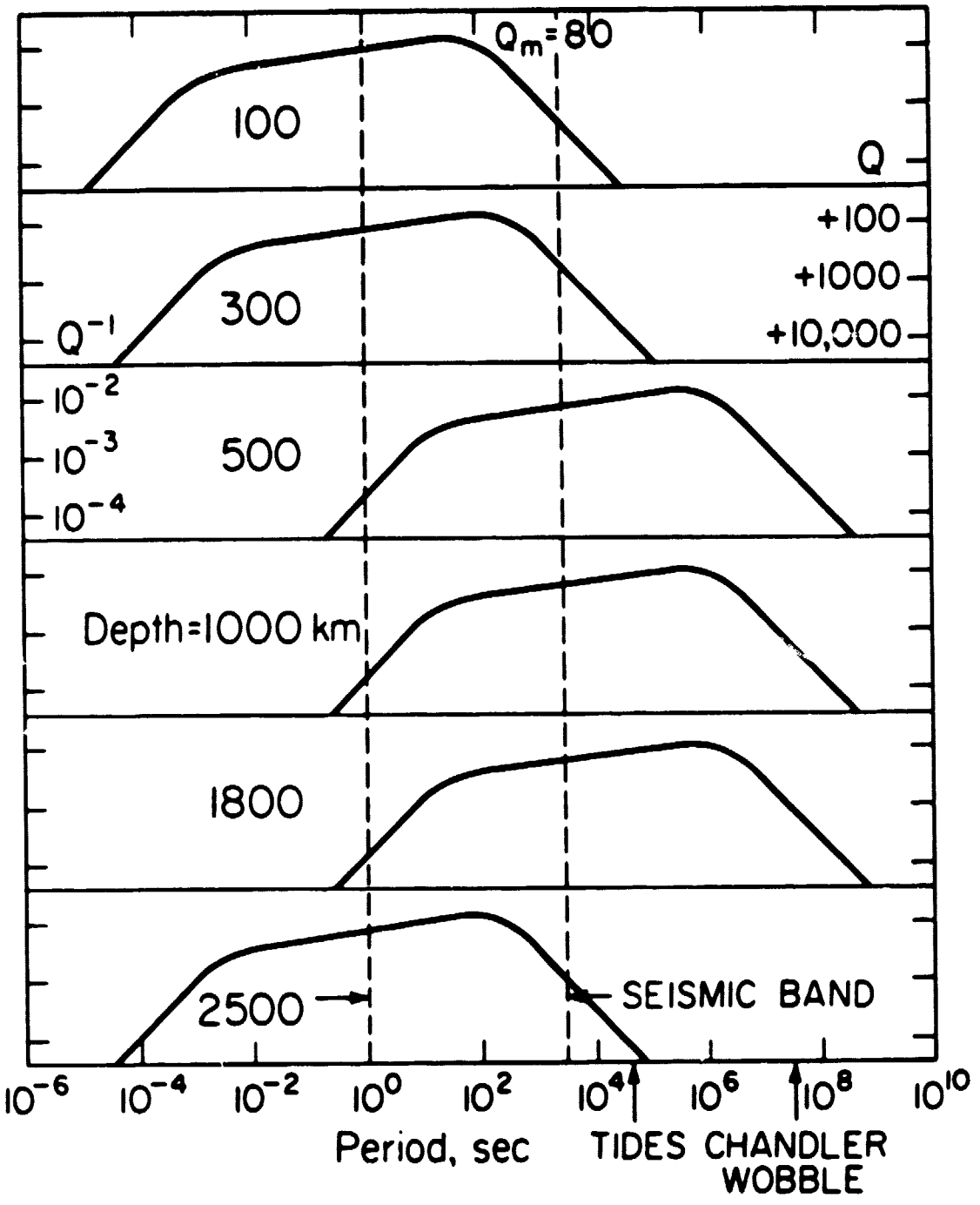
Q_m=80
100
Q
+100
+1000
+10,000
Q^{-1}
300
10^{-2}
10^{-3}
10^{-4}
500
Depth=1000 km
1800
2500
SEISMIC BAND
10^{-6}
10^{-4}
10^{-2}
10^{0}
10^{2}
10^{4}
10^{6}
10^{8}
10^{10}
Period, sec
TIDES
CHANDLER WOBBLE

Fig. 3

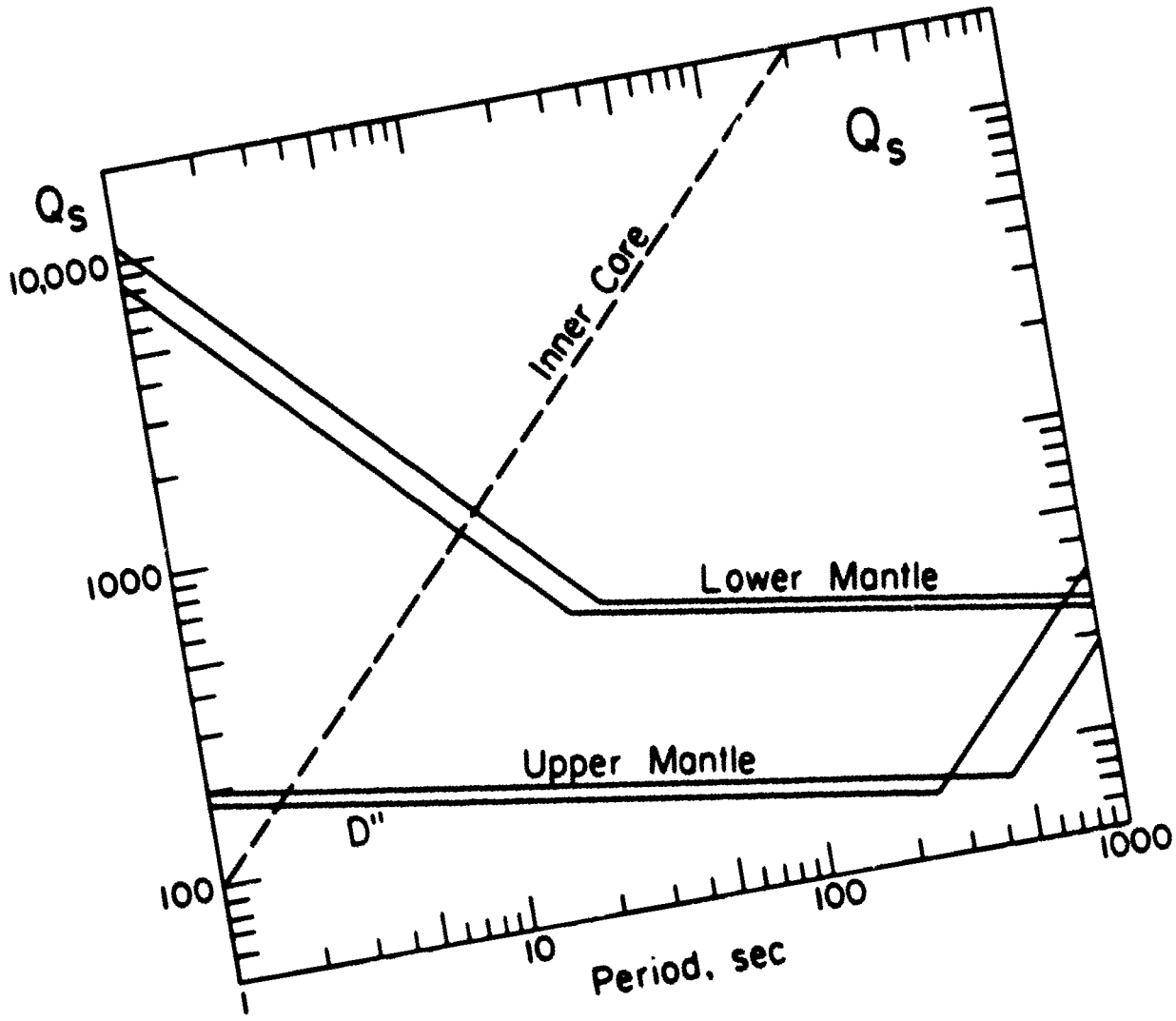
Q_S
10,000
1000
100
Q_S
Inner Core
Lower Mantle
Upper Mantle
D"
1
10
100
1000
Period, sec

Fig. 4

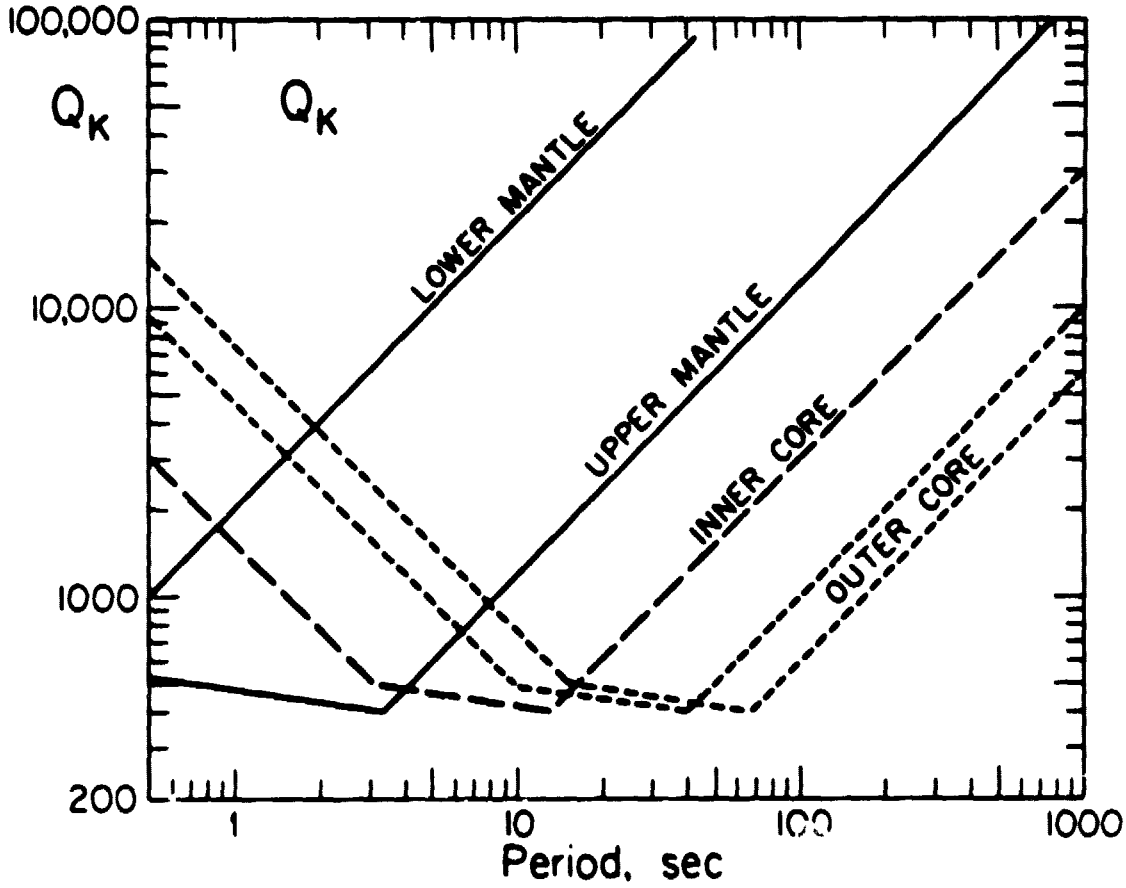
100,000
Q_K
Q_K
10,000
1000
200
LOWER MANTLE
UPPER MANTLE
INNER CORE
OUTER CORE
1
10
100
1000
Period, sec

Fig. 5

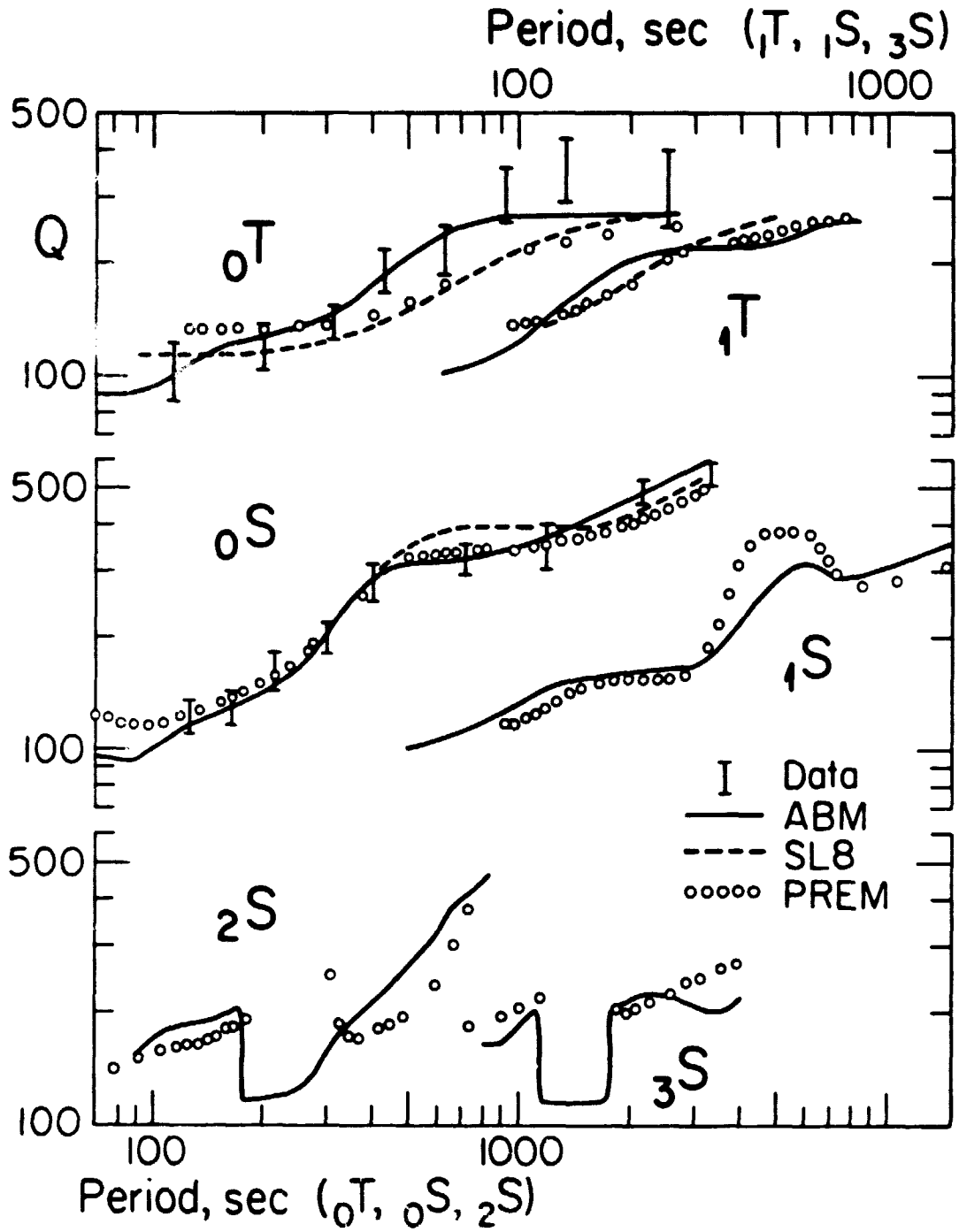
Period, sec ($_1$T, $_1$S, $_3$S)
100
1000
500
Q
$_0$T
$_1$T
100
500
$_0$S
$_1$S
100
I Data
ABM
SL8
PREM
500
$_2$S
$_3$S
100
100
1000
Period, sec ($_0$T, $_0$S, $_2$S)

Fig. 6

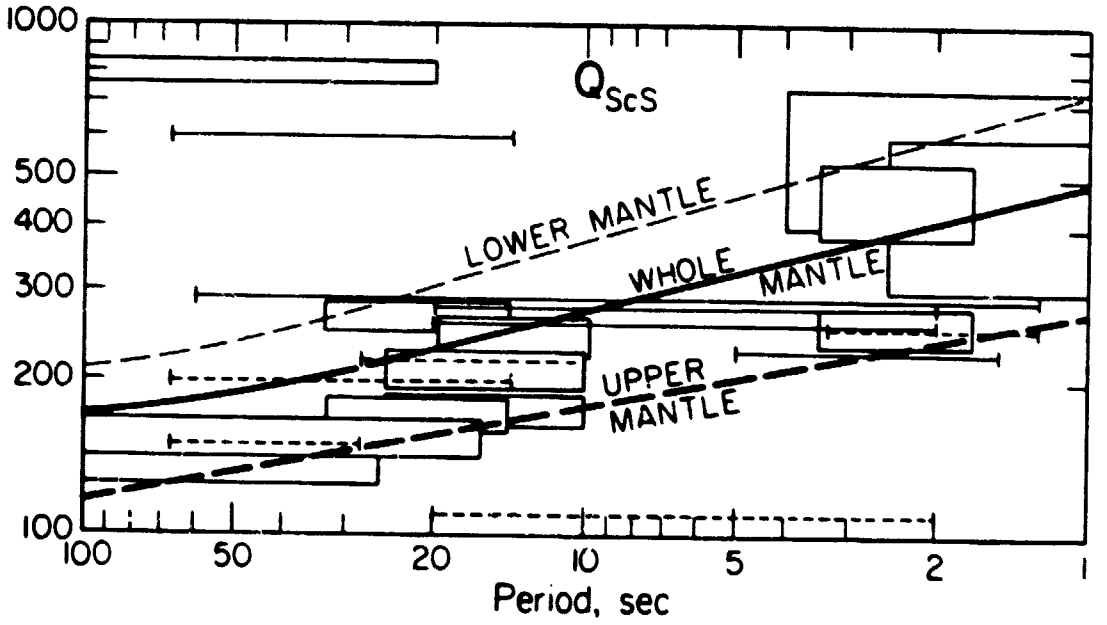
1000
500
400
300
200
100
Q_{ScS}
LOWER MANTLE
WHOLE MANTLE
UPPER MANTLE
100
50
20
10
5
2
1
Period, sec

Fig. 7